International Journal of Civil Engineering (2025) 23:43–55
https://doi.org/10.1007/s40999-024-01018-4

RESEARCH PAPER

Assessing Stray DC and AC Current-Induced Corrosion in Steel Fibre-Reinforced Concrete (SFRC) in Railway Tunnelling Construction

Kangkang Tang[1]

Received: 19 February 2024 / Revised: 24 June 2024 / Accepted: 5 July 2024 / Published online: 13 July 2024

Abstract
This paper discusses the uncertainties surrounding corrosion prompted by stray direct current (DC) and alternating current (AC) interferences. The influence of railway stray DC interference was simulated through cyclic potentiodynamic (CP) polarization in a simulated concrete pore solution. Steel fibres exhibit excellent resistance to stray DC perturbations up to 1.0 V (vs. OCP or Open Circuit Potential) in the absence of chloride. However, when the electrolyte contains 0.6 mol/L chloride, a reduced DC perturbation of 0.4 V (vs. OCP) was sufficient to initiate pitting corrosion, indicating decreased corrosion resistance. The stray AC interference was simulated by applying an AC perturbation test to the embedded steel fibres which were polarized in simulated concrete pore solution as well. This approach allows for the effect of steel fibre orientations under stray AC interferences to be assessed. Following the AC interference test, the Tafel polarisation test shows a stochastic corrosion pattern in the embedded steel fibres. Notably, there is a significant reduction in the corrosion potential (E_{corr}) and a corresponding increase in the corrosion current density (i_{corr}) observed in one of the fibres. Ongoing research is being conducted to explore the stochastic corrosion phenomena identified in this research. Boundary element modelling (BEM) results show that the maximum voltage drops between steel fibres arranged in various configurations closely correspond to experimental measurements. The computer simulation approach applied in this study has the potential to further advance the development of more valuable predictive tools in forecasting the corrosion behaviours of reinforced concrete exposed to stray currents under complex built environments.

Keywords Steel fibre reinforced concrete (SFRC) · Cyclic potentiodynamic (CP) · Potentiostat · Galvanostat

1 Introduction

Railway electrification stands as a significant carbon strategy in the UK. An electric train is estimated to consume at least 20% less power per passenger mile compared to a diesel-powered train [1]. Currently, only 39% of the national rail network in the UK is electrified, incorporating 600 V/750V direct current (DC) and 25 kV (50 Hz) alternating current (AC) traction power systems [2]. For an electrified railway, the power transmission is normally provided by the National Grid to the railway overhead contact line through a step-down transformer; the return circuit is usually achieved through the running rail which is connected to nearby substations [2]. Railway stray current refers to the electrical current that deviates from its intended pathway, flowing into surrounding metallic structures and eventually dissipating into the ground. Corrosion occurs at locations where the stray current exits from embedded metal surfaces. This process is schematically shown in Fig. 1. In the context of corrosion caused by stray direct current (DC), the extent of corrosion is primarily governed by the anodic overpotential (η_a), which serves as the propelling factor for steel corrosion. Bertolini [3] reported that an anodic overpotential (η_a) of 500–600 mV is required, establishing this range as both a necessary and ample condition for steel corrosion. It should be noted that steel reinforcement normally demonstrates good corrosion resistance. This can be attributed to the alkaline condition as a result of cement hydration reactions. Under such an alkaline condition, η_a is likely to result in oxygen evolution ($2H_2O \rightarrow O_2 + 4H^+ + 4e^-$) rather than steel dissolution ($F_e \rightarrow F_e^{2+} + 2e^-$) in the vicinity of the anodic area. Nevertheless, oxygen evolution can lead to

✉ Kangkang Tang
kangkangtang@gmail.com; Kangkang.tang@brunel.ac.uk

[1] Department of Civil and Environmental Engineering, Brunel University, London, UK

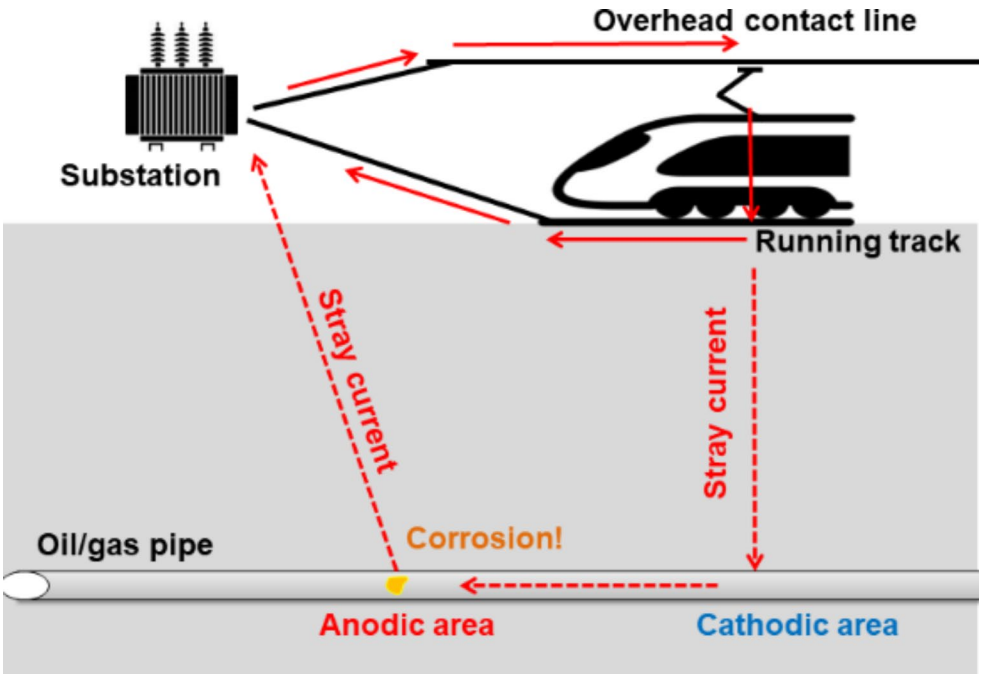

Fig. 1 Schematic of railway stray current-induced corrosion

the depletion of alkalinity and eventually the de-passivation of steel. Additionally, the hydrolysis products of iron ions ($F_e^{2+} + 2H_2O \rightarrow Fe(OH)_2 + 2H^+$) can further increase the acidity and thus enhance steel dissolution to accelerate the corrosion process. The minimum duration to result in spontaneous corrosion in reinforced concrete will be 14 months at an anodic current (i_a) of 0.1 mA/cm^2 under a chloride-free environment [3]. Nevertheless, when chloride is present, such as up to 0.2% chloride (by mass of cement) in concrete, the minimum current (i_a) needed to attain an equivalent corrosion rate decreases by an order of magnitude compared to conditions where chloride is absent [3]. This highlights the significant adverse impact of chloride on the corrosion resistance of steel reinforcement.

Stray AC-induced corrosion was identified considerably later when compared to stray DC-induced corrosion, even though 64% of the UK's electrified railway network relies on AC traction power systems [2]. Stray AC was perceived as less problematic when compared with stray DC, primarily due to a higher threshold current value for triggering steel reinforcement corrosion. Kuang and Cheng [4] reported that the AC threshold current density for corrosion could be 30 mA/cm^2 (60 Hz) under an alkaline environment. With the presence of 0.4% chlorides (by mass of cement), a reduced threshold current density of 5 mA/cm^2 was observed as the onset of steel reinforcement corrosion [5]. It is important to note that prior studies on pipelines have demonstrated that severe corrosion does not consistently take place in locations with the highest AC current density leakage [6]. Other factors, including pH and chloride levels, must also be considered when deciding the AC threshold current density.

In the construction of railway tunnel linings, steel fibres can be taken as a good alternative to traditional steel reinforcement, owing to their high compressive strength and superior fire resistance [1]. Moreover, research has indicated that the chloride threshold for corrosion in steel fibres surpasses that of conventional steel reinforcement [7]. The incorporation of steel fibres as a complete replacement for steel reinforcement also streamlines the concrete fabrication process by eliminating the necessity of constructing steel reinforcement cages. These advantages collectively ensure that railway tunnel lining construction could become a preferred application for steel fibre reinforced concrete (SFRC). The use of non-continuous steel reinforcement, such as steel fibres, in railway engineering dates back to the 1970s. During this time, steel fibre-reinforced shotcrete (spray concrete) was used in the construction of railway tunnels [8]. The incorporation of steel fibres into precast segmental linings came about at a later stage: the initial instance of a steel fibre-reinforced segmental lining tunnel was the London Heathrow Airport baggage tunnel, constructed in 1995 [8]. The Channel Tunnel Rail Link project in 2003 marked the first extensive use of steel fibre-reinforced concrete (SFRC) segments in railway projects [9]. Despite these previous applications, a significant research gap remains regarding the vulnerability of SFRC to stray current-induced corrosion. This issue was exemplified by the 'Guangzhou Metro Line' project in China, which initially intended to utilize SFRC as the primary tunnel lining material but ultimately abandoned this plan due to concerns regarding stray current-induced corrosion [10]. There is a pressing need to establish a validated methodology for assessing SFRC's

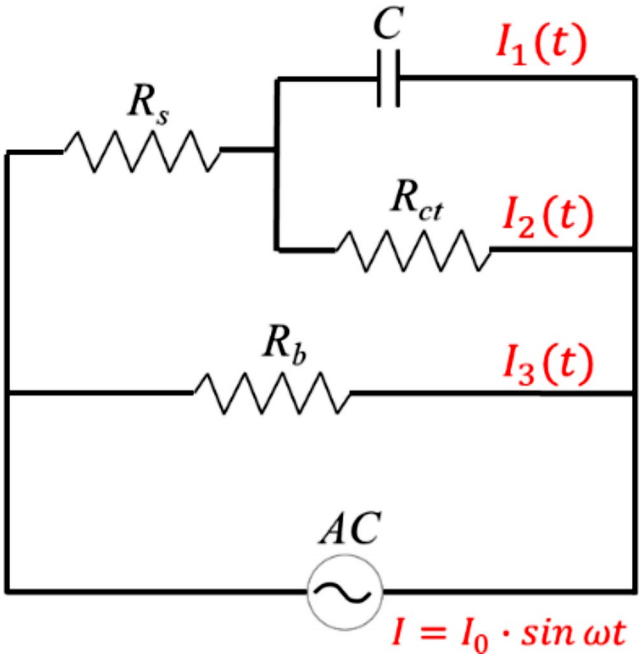

Fig. 2 Equivalent electrical circuit modelling of the steel-electrolyte interface under AC interference

susceptibility to stray current-induced corrosion, thereby enabling the secure deployment of steel fibres in such valuable applications.

The orientation of steel fibres plays a pivotal role in influencing the mechanical properties of concrete. As highlighted by Michels et al. [11], aligning steel fibres along the principal stress direction can lead to a substantial increase in concrete flexural strength, reaching nearly 30% with a fibre content of 40 kg/m³ – a content level akin to that employed in the construction of segments for the Chanel Tunnel project [12]. Various techniques have been developed to enhance the alignment of steel fibres along these critical stress directions [11, 13–16]. For instance, Kang et al. [16] improved steel fibre alignment through a secondary pumping and casting process following transport and initial compaction. Villar et al. [17] utilized an external magnetic field of 60 mT to enhance the alignment of steel fibres within a cement paste. An external magnetic field exerts magnetic torque on embedded steel fibres when there is an angle (φ) between the fibre orientation and the direction of the magnetic flux, effectively minimizing this angle (φ) to zero [17]. As such, this alignment enables the steel fibres to orient themselves in the direction of the principal stress, ultimately resulting in enhanced compressive strength of SFRC. However, it remains unclear whether the orientation of steel fibres has an impact on their electrochemical behaviour and, consequently, the durability of SFRC. This question persists despite a comprehensive review of the existing literature on the subject. This project has investigated the impact of steel fibre orientations on corrosion behaviour, marking a novel contribution to the research.

Tang [2, 18] reported key parameters influencing the corrosion rate of embedded steel reinforcement in the presence of stray AC conditions (Eq. 1). These parameters include the AC current value (I_0), AC angular velocity (ω), concrete bulk resistance (R_b), concrete resistance (R_s) between running track and steel reinforcements and concrete-steel interface properties. The concrete-steel interface properties are represented as charge transfer resistance (R_{ct}) and capacitance (C_{dl}) which can be determined through electrochemical impedance spectroscopy (EIS) analysis [18]. This information can be further depicted as an equivalent electrical circuit, as shown in Fig. 2, where I_2 signifies the Faraday current associated with steel dissolution. Equation (1) indicates that a decrease in either AC frequencies (ω), charge transfer resistance (R_{ct}), or double-layer capacitance (C_{dl}) will result in an escalation of in I_2, indicating a more severe corrosion process within the embedded steel. Figure 3 schematically illustrates the transient-state electrochemical reactions occurring in concrete with discontinuous steel fibres under the influence of stray AC current. These established models have laid the groundwork for further exploration of the impact of steel fibre orientation on the charge transport mechanism under stray AC conditions, which is further discussed in Sect. 2.2 of this paper.

$$I_2(t) = \frac{b}{\sqrt{\omega^2 + a^2}} \sin(\omega t - \theta) + \frac{b \cdot \omega}{\omega^2 + a^2} \cdot e^{-\mathrm{at}} \tag{1}$$

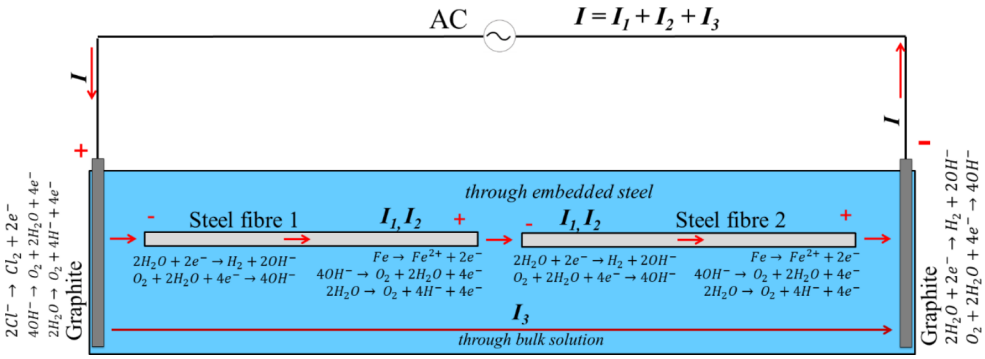

Fig. 3 Schematic of transient-state electrochemical reactions in concrete with discontinuous steel fibres induced by stray AC current

$$\text{Where}: a = \frac{R_b + R_s + R_{ct}}{C_{dl} \cdot R_{ct} \cdot R_b + R_s \cdot C_{dl} \cdot R_{ct}},$$
$$b = \frac{R_b \cdot I_0}{C_{dl} \cdot R_{ct} \cdot R_b + R_s \cdot C_{dl} \cdot R_{ct}}, \theta = arctan\frac{\omega}{a}$$

The electrochemical performance of a steel specimen can be assessed by conducting a polarization test under either controlled the peak electric voltage (e.g. potentiostatic) or current (e.g. galvanostatic) [1, 19]. For reinforced concrete, determining polarization curves (or *E-i* curves) for steel in a solid electrolyte like concrete can be challenging. It is therefore common practice to determine the *E-i* curves in an aqueous solution that simulates the concrete pore solution. For instance, when investigating the corrosion of steel reinforcement, many researches [20–22] have been conducted using saturated $Ca(OH)_2$ solution to simulate the concrete pore solution. Using an aqueous electrolyte also facilitates determining the critical chloride content, or chloride threshold level, for reinforced concrete. Hausmann [23], Saremi and Mahallati [24] have reported that the chloride threshold level for ordinary steel reinforcement to corrode was 0.6 which represents the active $[Cl^-]/[OH^-]$ ratio in a concrete pore solution. In this project, saturated $Ca(OH)_2$ solution was used to approximate the pore solution in hydrated concrete. It is worth mentioning that the resistivity of a solid electrolyte such as concrete may affect the anodic behaviour during corrosion reactions, particularly when the reaction speed (or corrosion rate) is governed by the anodic reactions. Additionally, on the cathodic side, a solid electrolyte can impact oxygen transport and consequently, the cathodic reaction process. The impact of concrete resistivity on the corrosion characteristics of steel fibres was discussed separately by the author [18].

In addition to experimental work, computer simulations have been increasingly used for predicting the corrosion behaviour in reinforced concrete. For instance, Brenna et al. [25] used finite element modelling (FEM) to examine stray DC current development in a tramway tunnel. In comparison to FEM, boundary element modelling (BEM), which requires discretizing only the domain boundaries, offers the advantage of significantly reducing the total number of elements. This efficiency enhancement was demonstrated by Cui et al. [26] in their analysis of a 1.6 km pipeline, where only the pipeline itself (excluding the surrounding soil) was discretized. BEM has been employed in this project, as discussed in Sect. 2.3, to study the corrosion behaviour of embedded steel fibres, representing a novel application of this method in concrete research.

2 Research Methodologies

In this project, the corrosion tendencies of 76 mm-long, 1 mm-diameter steel fibres, produced through the cold drawing process of mild steel with hooked ends, were examined. To simulate stray DC interference, the cyclic potentiodynamic (CP) polarization technique was used to simulate stray direct current (DC) interference which applied a continuous DC voltage to the working electrode (e.g. steel fibre) to obtain the polarization curves (*E-i* curves) to assess its corrosion resistance. To simulate stray AC interference, an AC polarization test was conducted by applying an AC current (200 mA, 50 Hz) between two graphite plates. This test polarized embedded steel fibres within a high-density upholstery foam beam saturated with a simulated concrete pore solution, replicating the porous structure of concrete [1]. This setup allowed exploration of diverse steel fibre orientations' responses to stray AC interferences, as detailed in Sect. 2.2. All steel fibres were ground by 2000 grit emery paper and rinsed in deionized water prior to testing. Complementing experimental methods, computer simulations using boundary element modelling (BEM) were employed to validate the study's findings.

2.1 Measurement of Steel Fibre Corrosion Resistance to DC Interference

Before the DC interference test, individual steel fibres were securely attached to PVC-coated copper wires. This attachment was reinforced with a hot melt polymer adhesive, serving a dual role of protecting against corrosive deterioration and ensuring an approximate exposed surface area of 2.2 cm^2 for each steel fibre being investigated. The cyclic potentiodynamic (CP) polarization test was then conducted using a 3-elecrode electrochemical cell as seen in Fig. 4 (a) (b). The electrode potential was measured relative to an Ag/AgCl reference electrode (RE), which has a filling solution comprising 3% KCl. The influence of ohmic drop, resulting from the current flow between the anode and cathode, can be substantial when dealing with solid electrolytes like concrete with a relative humidity below 70% [3]. In the case of railway segmental linings, which are a primary application of steel fibres in this study, the relative humidity is often much higher, exceeding 95%. Such a high humidity was considered in this study by using aqueous electrolytes to simulate concrete pore solutions which was based on the saturated $Ca(OH)_2$ solution. NaCl was introduced at varying concentrations (i.e. 0, 0.3 and 0.6 mol/L) to replicate diverse working conditions. The latter, i.e. 0.6 mol/L, represents seawater salinity.

All electrolytes were prepared using deionized water and the NaCl used is of analytical grade. A high-density

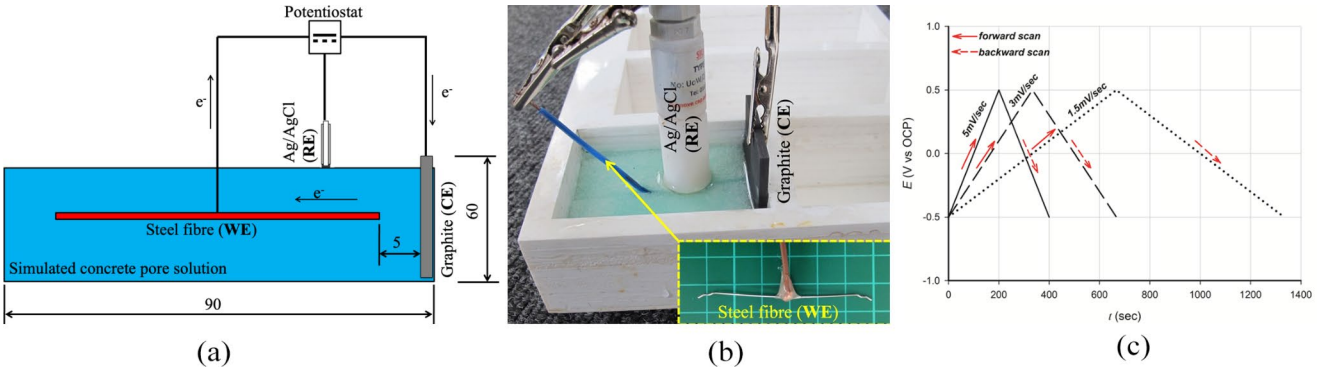

Fig. 4 CP polarization test (all units in mm unless otherwise stated). (**a**) Schematic of CP polarization test cell. (**b**) Photograph of CP polarization test cell. (**c**) CP polarization test potential-time curve

upholstery foam beam was utilized to imitate the porous nature of concrete. This foam beam absorbed the aqueous electrolytes as discussed above, approximating the porous structure of concrete. A Gamry Interface 1000E potentiostat was used to measure the current passing between the working electrode (specifically, the steel fibre) and a graphite counter electrode (CE) measuring 40 × 50 × 2 mm. The following parameters of CP polarization were considered:

- Varying CP polarization scanning rate: 1.5, 3 and 5 mV/sec, as seen in Fig. 4 (c), with a CP voltage between − 0.5 and 0.5 V (vs. OCP) in the saturated $Ca(OH)_2$ solution containing 0, 0.3 and 0.6 mol/L NaCl.

A conditioning time of 15 min was maintained before the CP polarization test, allowing for the open circuit potential (OCP) to be measured. In order to assess the consistency of the CP polarization outcomes, three parallel samples were used for each test, under a constant temperature of 20 °C. The subsequent CP polarization curves and findings are elaborated upon in Sect. 3.1.

A heightened DC voltage, reaching a maximum of 1.5 V (versus OCP), was applied to recently prepared steel fibres to simulate DC interference. This was conducted to explore the potential for corrosion due to stray DC currents at high voltages, in an environment free from chloride exposure. The experimentation involved a consistent voltage scanning rate of 3 mV/sec. Further elaboration on these findings is provided in Sect. 3.1.

- Varying CP polarization voltages: 0.5, 1.0 and 1.5 mV (vs. OCP) in the saturated $Ca(OH)_2$ solution.

2.2 Measurement of Steel Fibre Corrosion Resistance to AC Interference

The stray AC interference test was developed using a galvanostatic method characterized by a controlled peak current flow (I_0). The Gamry Interface 1000E potentiostat, equipped with Gamry's Virtual Front Panel (VFP600) software package, functions as the galvanostat. It drives constant an AC current between two auxiliary graphite electrodes while simultaneously measuring the voltage drop between the embedded steel fibres. This technique enables the simultaneous polarization of two steel fibres positioned between auxiliary graphite electrodes (40 × 50 × 3 mm) when subjected to a 200 mA (50 Hz) AC current for one hour. Two different steel fibre orientations, as presented in Fig. 5, were investigated to gain insights into the corrosion effects. In the AC interference test, a consistent concentration of 0.3 mol/L NaCl was maintained within the simulated concrete pore solution. Two parallel samples were used for each test, under a constant temperature of 20 °C. The voltage measurement carried out between two steel fibres was undertaken to confirm the predicted voltage drop between them as indicated by the computer simulation. This is discussed in Sect. 3.3.

After the 1-hr AC interference, all tested steel fibre samples were rinsed using de-ionized water. A Tafel polarization test was then conducted to each steel fibre in a 3-electrode cell (Fig. 6) using freshly prepared saturated $Ca(OH)_2$ solution as the electrolyte. The steel fibre was used as the working electrode (WE) and its electrode potential was measured with regards to a silver/silver chloride (Ag/AgCl) reference electrode (RE, with filling solution 3% KCl) which was placed on the top surface of the foam beam. During Tafel polarization, a constant potential scanning rate, 1 mV/sec, was applied to the WE and the potential ranged of -250 to + 250 mV (vs. OCP). Such a scanning rate allowed the nonlinear correlation between externally applied potential (E) and the current density i ($i = I/A$)

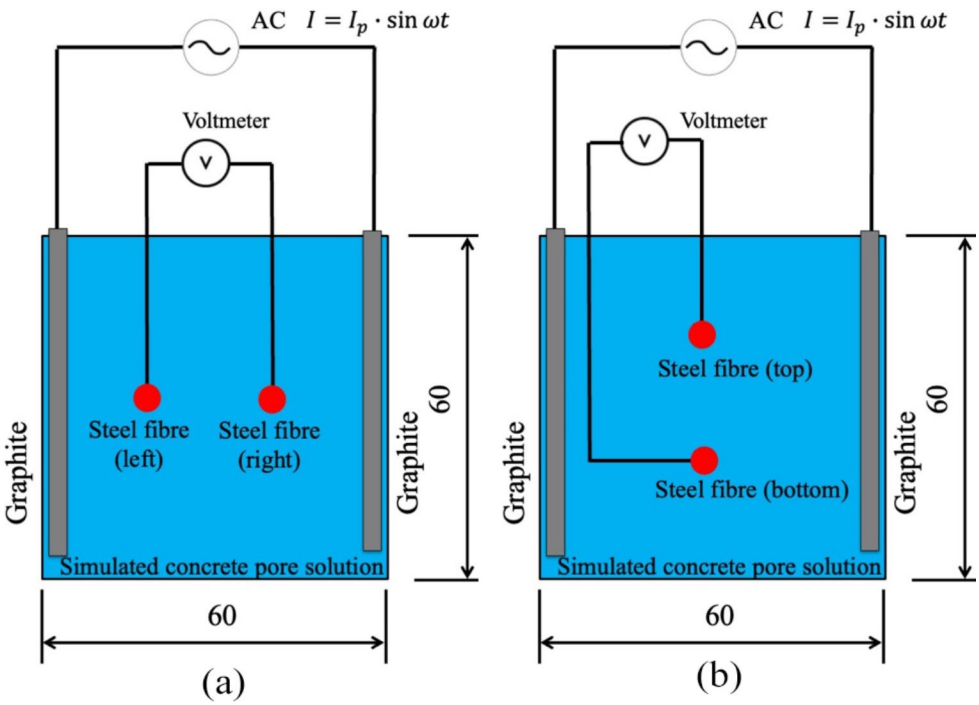

Fig. 5 AC interference test (all units in mm unless otherwise stated). (**a**) Steel fibre position 1: back-to-back arrangement. (**b**) Steel fibre position 2: top-bottom arrangement

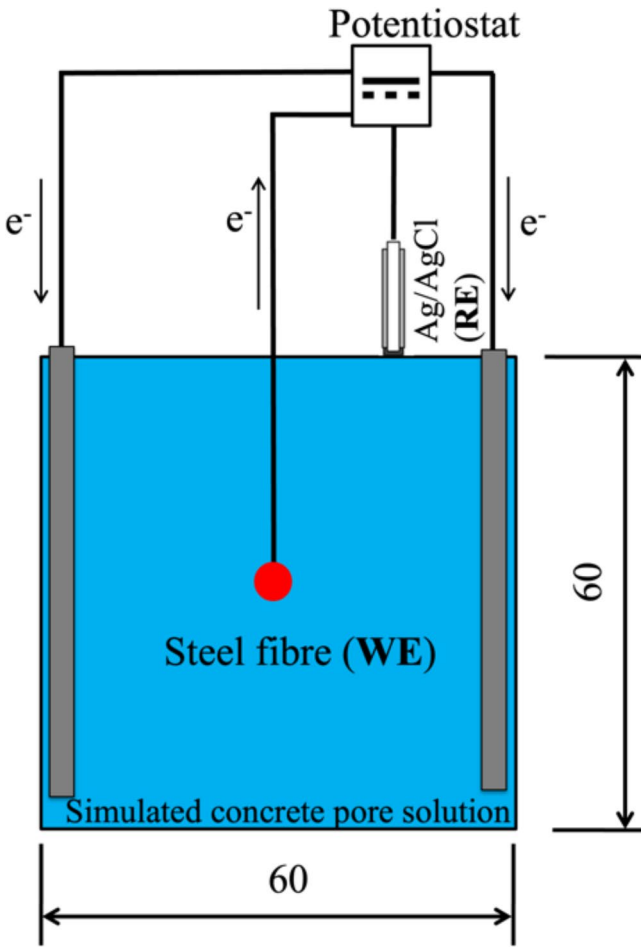

Fig. 6 Tafel polarization test (all units in mm unless otherwise stated)

response to be measured, and this was selected to achieve a balance between testing efficiency and accuracy, as detailed in Sect. 3.1, while discussing the CP polarization results. Different from CP polarization which typically covers a wider potential range to gain insights into various stages of a material or system's behaviour (such as localized corrosion, pitting, and passivation), akin to how metals respond to stray DC interference, Tafel polarization involves applying a small voltage perturbation around the Open Circuit Potential (OCP), and this allows for the determination of the anodic and cathodic reaction rates within this specific voltage range. In summary, Tafel polarization primarily focuses on assessing critical electrochemical parameters related to corrosion kinetics, which ultimately inform the prediction of long-term corrosion rates [1]. It has been used in this study to estimate the long-term corrosion rate of steel fibres following the AC interference test.

During the Tafel polarization test, electric current flow between the WE and two counter electrodes (CE), i.e. two $40 \times 50 \times 3$ mm graphite plates, was measured by the Gamry potentiostat. Tafel slope analysis was conducted to determine the corrosion current density ($i_{corr} = I_{corr}/A$) and corrosion potential (E_{corr}) based on a nonlinear regression between the applied potential (E) and the current density i ($i = I/A$), or the Butler-Volmer equation (Eq. (2)), using Gamry Echem Analyst software [27]. The corrosion rate (CR) can then be estimated based on the interpreted i_{corr} value using Eq. (3) [28]. For a more detailed exploration of results and discussions, please refer to Sect. 3.2.

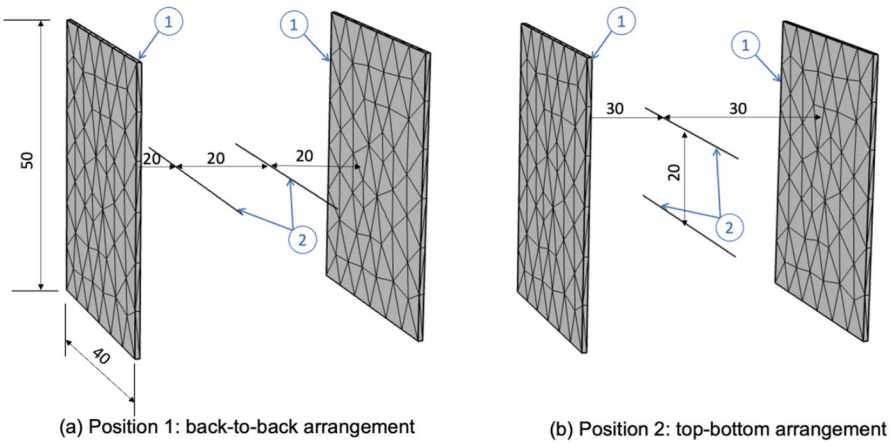

Fig. 7 Boundary element modelling for 3 cells shown in Fig. 5 (① graphite plate, ② steel fibre, all units in mm)

$$I = I_{corr}\left[\exp\left(\frac{\mathrm{E}-E_{corr}}{\beta_a}\right) - \exp(-\frac{\mathrm{E}-E_{corr}}{\beta_c})\right] \quad (2)$$

$$CR = \frac{Ki_{corr}EW}{\rho} \quad (3)$$

2.3 Computer Simulation

In order to have a better understanding of the electric field developed in an electrolyte containing discrete steel fibres, numerical modelling was conducted using COMSOL Multiphysics 5.4. The COMSOL model geometry, representing the two AC interference tests presented in Fig. 5, is shown in Fig. 7. The 76 mm long steel fibre was discretized into 1D 'pipe' elements using boundary element method (BEM), with a maximum BEM element size of 4 mm. Such pipe elements were selected for steel fibres because they can better model the skin effect when an alternating electric current is transmitted, i.e. the current density is much higher near the surface under an AC condition [29]. For more comprehensive details regarding BEM pipe elements, please refer to [30]. Auxiliary graphite electrodes (40×50×3 mm) were meshed into 2D tetrahedral elements using finite element method (FEM), with a maximum element size of 8.3 mm. Electrolytes were considered as a semi-infinite domain with the electrolyte's top surface in contact with air. An AC current ($I = I_0 \cdot \sin\omega t$, $I_0 = 200mA$ *and* $\omega = 50Hz$), same as that used in the AC interference test, was applied between the auxiliary graphite electrodes.

The kinetics of electrochemical reactions taking place on the steel surface were considered using polarization curves derived from Tafel polarization results. These steel polarization curves, also known as *E-i* curves, were determined at various chloride concentrations and then employed in the BEM model through a piecewise linear interpolation method [26]. In this approach, the polarization curve is approximated using a series of straight lines, as depicted in Fig. 8. The root mean square error (RMSE), which quantifies the discrepancy between the actual measurements (*E-i*) and those acquired from the linear piecewise simulation, is also shown in Fig. 8.

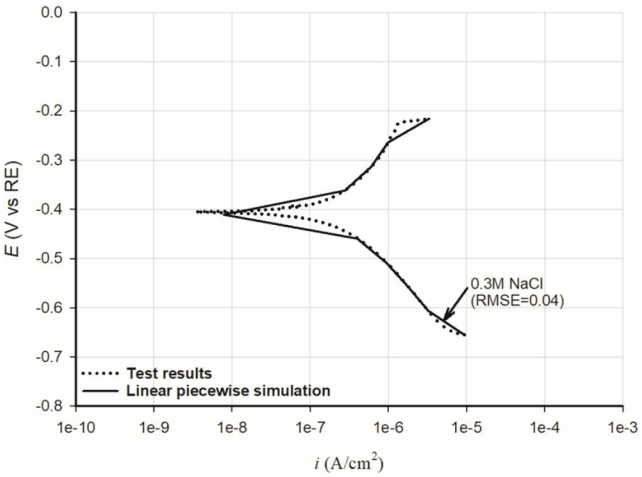

Fig. 8 Linear piecewise approximation of the measured polarization (*E-i*) curve

Electrical conductivity (S/m) measures a material's capacity to conduct an electric charge. For the saturated calcium hydroxide solution, an electrical conductivity value of 0.73 S/m was used in this study based on published data [31]. The NaCl solution, with its higher salinity and increased presence of dissolved ions (Na^+ and OH^-), exhibits much higher electrical conductivity. A value of 2.4 S/m for the conductivity of a 0.3 mol/L NaCl solution was sourced from published data [32]. Furthermore, the electrical resistivity of embedded steel fibres and auxiliary graphite electrodes was determined as 4.6×10^{-7} and 2.5×10^{-6} Ω·m, respectively, in accordance with published findings [33, 34]. The voltage drop between discrete steel fibres (*E*) was experimentally ascertained and discussed in Sect. 3.2, serving as a validation point for the numerical model, and this is discussed in Sect. 3.3.

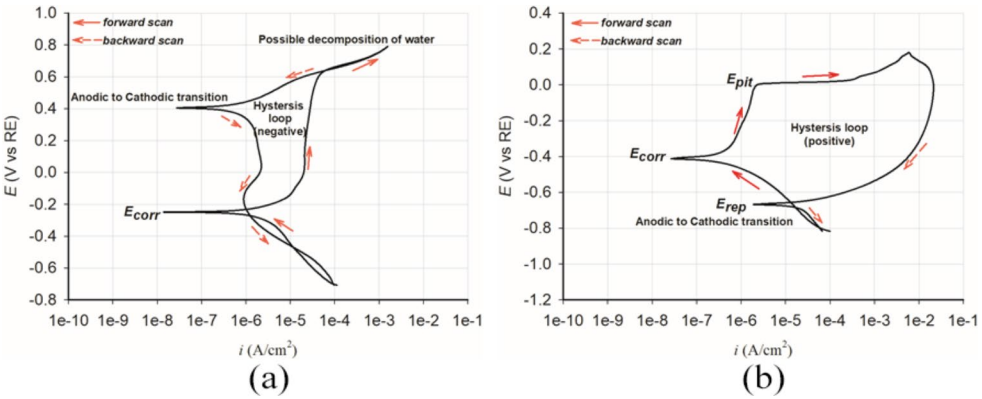

Fig. 9 Observation of two CP polarization curve patterns. (**a**) CP polarization curve type 1: negative hysteresis loop (0.0 mol/L NaCl in saturated $Ca(OH)_2$ solution). (**b**) CP polarization curve type 2: positive hysteresis loop (0.6 mol/L NaCl in saturated $Ca(OH)_2$ solution)

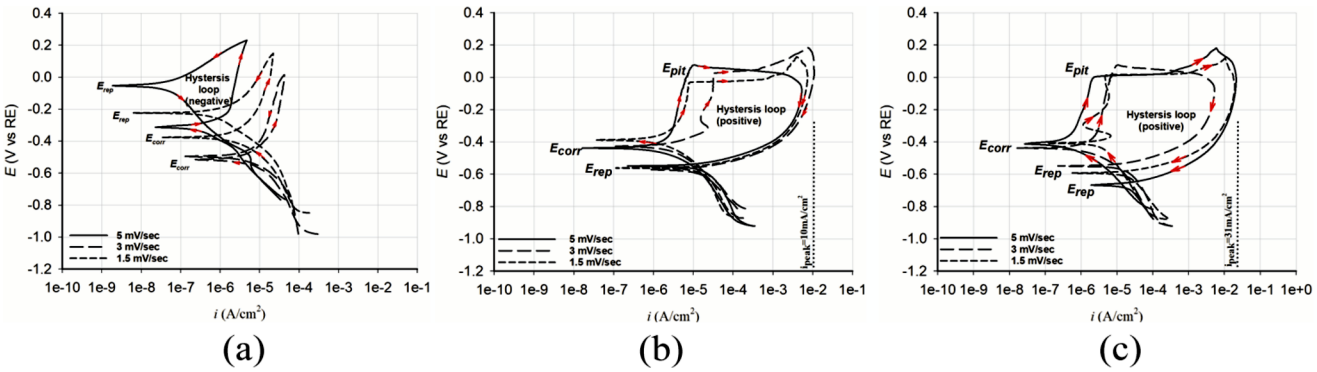

Fig. 10 CP polarization results – effects of chloride concentrations and scanning rates on *E-i* curves. (**a**) 0.0 mol/L NaCl in saturated $Ca(OH)_2$ solution. (**b**) 0.3 mol/L NaCl in saturated $Ca(OH)_2$ solution. (**c**) 0.6 mol/L NaCl in saturated $Ca(OH)_2$ solution

3 Results and Discussion

3.1 Corrosion Behaviour of Steel Fibre Subject to Stray DC Interference

CP polarization results can be presented as curves between the electrode potential E (vs. Ag/AgCl RE) and the current density i ($i = I/A$), plotted on a logarithmic scale. In this investigation, two distinct patterns of CP polarization curves were observed: specifically identified as type 1 (Fig. 9 (a)) and type 2 (Fig. 9 (b)). Both of these patterns exhibit the corrosion potential (E_{corr}) during the forward or positive scan. At E_{corr}, the rate of the anodic reaction matches that of the cathodic reaction, leading to no net current flow out of the system. For CP polarization curve type 1 (Fig. 9 (a)), the current densities measured during the reverse scan were lower than those measured during the forward scan under the same magnitude of external voltage (E). This negative hysteresis condition indicates that the steel was under a good protection by the steel passive layer even subject to a positive voltage, leading to reduced current densities [35]. The type 2 CP polarization curve, as observed in Fig. 9 (b), displays a positive hysteresis loop or the current densities during the reverse scan are higher than those measured during the forward scan. Alongside this, pitting potential (E_{pit}) was observed during the forward scan, and it was associated with the breakdown of the protective steel passive layer. In addition to the positive hysteresis loop and E_{pit}, repassivation potential (E_{rep}) was observed as the potential at which the current density decreases significantly and stabilises during the reverse scan, indicating that the passive film has reformed. Since E_{rep} was lower than the corrosion potential (E_{corr}), this indicates an instance of active corrosion. In this scenario, the stability of the steel's passive layer was compromised even in the absence of an externally applied DC voltage (E), resulting in the initiation and growth of new pits.

Figure 10 (a) shows that the steel fibres were under a good protection (resembling type 1 CP polarization, as seen in Fig. 9 (a)), in the absence of NaCl in the electrolyte. In contrast, the presence of 0.3 mol/L *NaCl* in the electrolyte led to active corrosion in steel fibres, as seen in Fig. 10 (b). Notably, Fig. 10 (b) shows that E_{pit} became measurable even under a rapid scanning rate of 5 mV/sec, signifying ample time for pit initiation and nucleation, even at such a high scanning rate. This observation persists with a high chloride concentration electrolyte, specifically at 0.6 mol/L as depicted in Fig. 10 (c). Here, the effect of scanning rates on the measured CP polarization curves proved to be

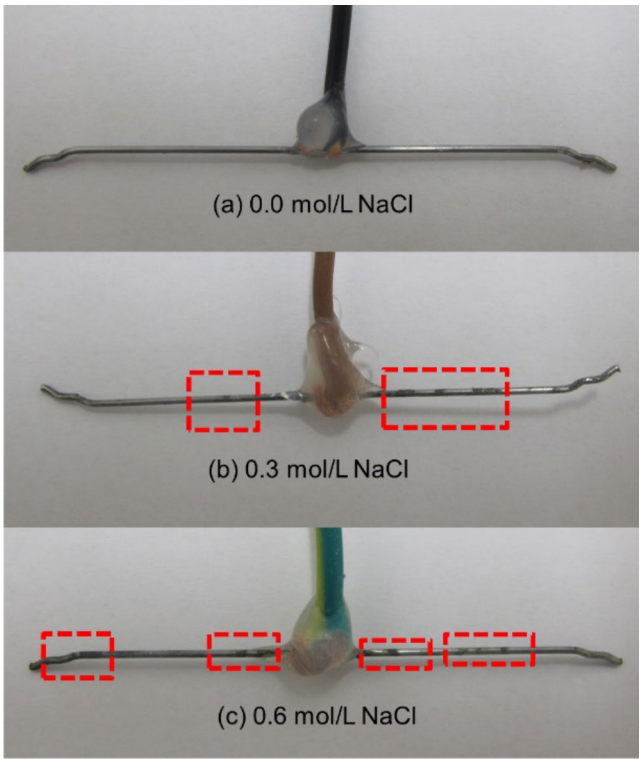

Fig. 11 Steel fibre samples after CP polarization tests (observed corroded areas highlighted in red dashed lines)

negligible, with curves obtained at various scanning rates displaying striking similarities.

Both Fig. 10 (b) and Fig. 10 (c) exhibit positive hysteresis during the reverse scan (akin to type 2 CP polarization, as seen in Fig. 9 (b)), with a larger area encompassed by the hysteresis loop obtained at a slower scanning rate of 1.5 mV/sec. This suggests that the steel fibre surface encounters greater difficulty in repassivation at such a slow scanning rate. Alternatively, a slower scanning rate permits pits to continue growing and propagating at an anodic voltage, aligning with the observations made by Esmailzadeha et al. [35]. A slow scanning rate, e.g. 1.5 to 3 mV/sec, also allows for the agglomeration of chloride in the pits which may better replicate railway stray DC interference. In comparison to Fig. 10 (b), Fig. 10 (c) reveals that E_{pit} shifted to more negative values under a highly concentrated chloride condition, i.e. 0.6 mol/L. As E_{pit} is associated with the breakdown of the steel passive layer, this shift implies increased corrosive damage to the steel fibre surface. Figure 10 (c) also demonstrates that similar E_{pit} at different scanning rates, suggesting that the scanning rate, up to 5 mV/sec, did not significantly impact charge transfer at the steel-electrolyte interface. This phenomenon might be attributed to the ample presence of chloride ions in the 0.6 mol/L NaCl electrolyte. Furthermore, peak current densities (i_{peak}) reaching up to 31 mA/cm² during the reverse scan, indicating a severe corrosive attack on the steel fibre surface. This observation is corroborated by visual inspections of the working electrode (i.e. steel fibre) following CP polarization.

Figure 11 illustrates the precipitation of corrosion products on the steel surface, likely attributed to the formation of magnetite (Fe_3O_4) due to the limited availability of oxygen in the electrolyte [36]. In summary, steel fibres exhibit good corrosion resistance to stray DC perturbations in the absence of chloride. With 0.6 mol/L chloride in the electrolyte, a reduced but still significant DC perturbation of 0.4 V (vs. OCP) was required to initiate pitting corrosion, indicating reduced corrosion resistance (Fig. 12 (c)). Figure 12 also shows consistent steel polarization curves obtained at a scanning rate of 5 mV/sec. This, coupled with an E_{pit} value comparable to those obtained at lower scanning rates (as seen in Fig. 10), suggests that a scanning rate of up to 5 mV/sec is apt for evaluating the breakdown of the steel's passive layer in the presence of ample chloride ions (e.g. 0.6 mol/L) within the electrolyte. This finding is important for future research as it enables more efficient investigations without compromising crucial and meaningful results at an accelerated scanning rate.

To further investigate the corrosion resistance of steel fibres under a higher DC voltage, CP polarization was

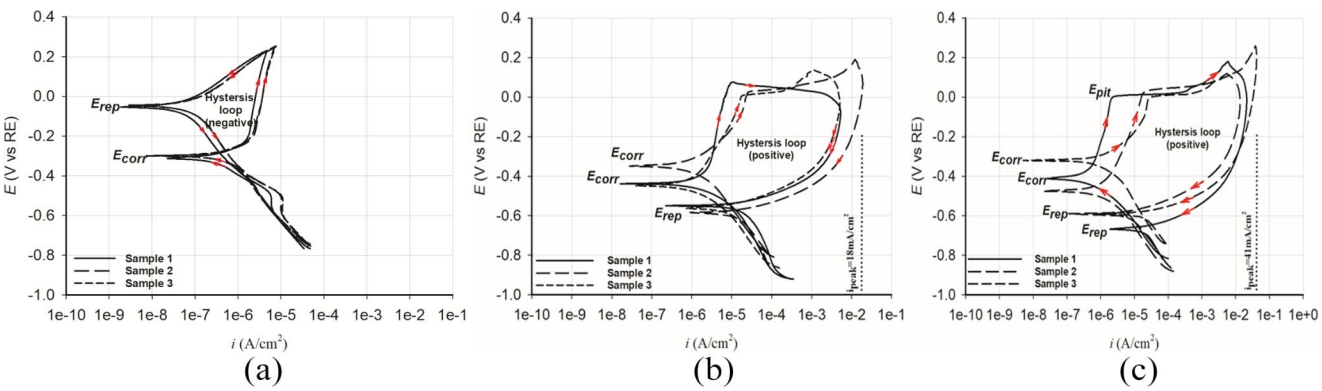

Fig. 12 3 parallel CP polarization test results (scan rate: 5 mV/sec). (**a**) 0.0 mol/L NaCl in saturated $Ca(OH)_2$ solution. (**b**) 0.3 mol/L NaCl in saturated $Ca(OH)_2$ solution. (**c**) 0.6 mol/L NaCl in saturated $Ca(OH)_2$ solution

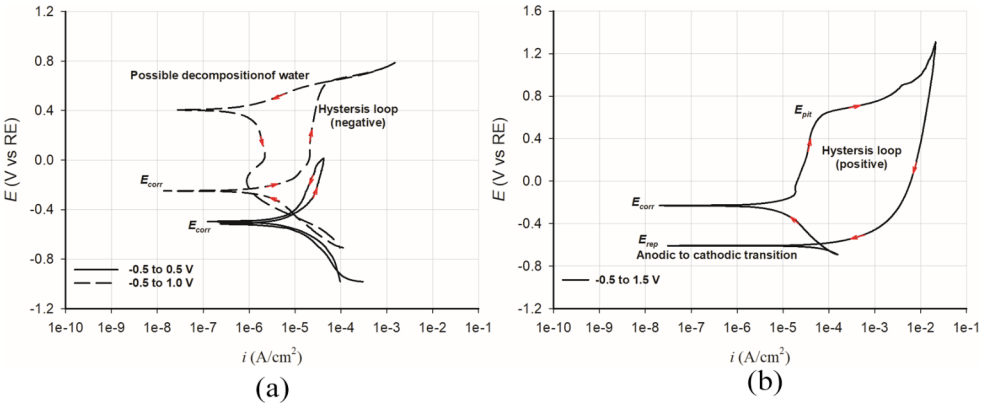

Fig. 13 CP polarization results – *E-i* curves under different magnitudes of peak voltage perturbation (chloride-free). (**a**) CP voltages between − 0.5 and 0.5 V; -0.5 and 1.0 V (vs. OCP). (**b**) CP voltages between − 0.5 and 1.5 V (vs. OCP)

conducted using freshly prepared steel fibre samples and electrolytes, with the peak DC voltage increased to 1.0 and 1.5 V respectively. Figure 13 (a) demonstrates that the steel fibre maintained effective protection (resembling a type 1 CP polarization pattern, as observed in Fig. 9 (a)) when subjected to a positive voltage of up to 1.0 V (vs. OCP). However, at a peak DC voltage of 1.5 V (vs. OCP), a notable E_{pit} was observed, indicating the breakdown of the steel's passive layer (Fig. 13 (b)). Alternatively, this suggests that the repassivation effect on the steel was weaker than the destructive impact of the external voltage (E), resulting in enhanced corrosion reactions.

The presence of stray currents introduces variations in the corrosion behaviour of embedded steel fibres, influenced by factors such as alkaline and chloride content. Therefore, it is crucial to examine stray current-induced corrosion in both a chloride-free, uncontaminated setting and a chloride-contaminated environment. Under a chloride-free environment, a small positive voltage up to 1.0 V (vs. Ag/AgCl) can lead to oxygen evolution ($2H_2O \rightarrow 4H^+ + 4e^- + O_2$) at the anodic area alongside a negative hysteresis loop observed in the *E-i* curves (as seen in Fig. 10 (a)). The oxygen evolution also produces acidity which can neutralize the alkalinity at the steel-concrete interface and eventually lead to the breakdown of the steel passive layer. A positive hysteresis loop observed under a higher voltage > 1.0 V (vs. Ag/AgCl) indicates steel dissolution ($Fe \rightarrow Fe^{2+} + 2e^-$). Figure 13 (b) shows that a driving voltage of at least 1.3 V (vs. Ag/AgCl) is required for the corrosion current density to exceed 20 mA/cm^2. This indicates that a significant steel corrosion rate can still be achieved subject to a higher external positive voltage which serves as the predominant driving force for steel fibre corrosion in a chloride-free environment. The presence of chlorides diminishes this driving force required to reach similar corrosion current density. Figure 12(b) reveals a positive hysteresis loop, indicating steel dissolution ($Fe \rightarrow Fe^{2+} + 2e^-$) at the anodic area. With a considerably lower driving voltage of 0.17 V (vs. Ag/AgCl), the anodic current density reaches 18 mA/cm^2.

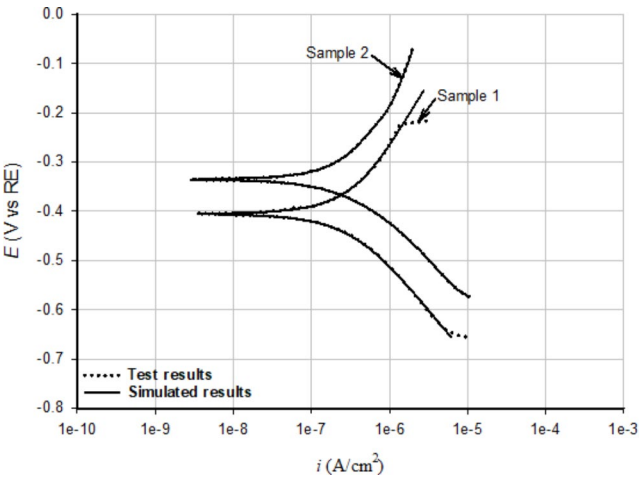

Fig. 14 Tafel polarization results prior to AC interference (0.3 mol/L NaCl)

This is despite that a much higher voltage of 0.5 V (vs. Ag/AgCl) was required to reach *Epit*.

3.2 Corrosion Behaviour of Steel Fibre Subject to Stray AC Interference

As discussed in Sect. 2.2, the AC interference test was conducted using a 200 mA, 50 Hz current to simulate railway stray current interferences. Figure 14 shows the Tafel polarization curves obtained from two steel fibre samples prior to the AC interference test. These Tafel polarization outcomes are represented as curves depicting the electrode potential E (vs. RE) against the total current density i ($i = I/A$), presented on a logarithmic scale. A nonlinear regression analysis, employing the Butler-Volmer equation (Eq. (2)), was performed using Gamry Echem Analyst software [27]. The best-fit curves are depicted in Fig. 14 as dashed lines and best fit parameters, including E_{corr},i_{corr},β_a and β_c, are presented in Tables 1 and 2. Figure 14 illustrates that both samples exhibit similar polarization curves prior to the introduction of AC interference.

Table 1 Tafel polarization results (before AC interference)

	E_{corr} (mV)	β_a (V/dec)	β_c (V/dec)	i_{corr} ($\mu A/cm^2$)	CR (mm/year)
Sample 1	-331	0.221	0.134	0.096	0.001
Sample 2	-335	0.282	0.151	0.128	0.001

After the 1-hour AC interference test, the Tafel polarisation test was conducted to the steel fibres, and the results are presented in Fig. 15. The Tafel polarisation curves obtained after the AC interference test exhibit a stochastic corrosion pattern in the two embedded steel fibres. Notably, there is a significant decrease in the corrosion potential (E_{corr}) and a corresponding increase in the corrosion current density (i_{corr}) in only one of the two fibres. This distinctive pattern signifies severe corrosion on only one of the fibres. Subsequent calculations to determine the corrosion rate (CR), as shown in Table 2, reveal a tenfold increase in CR for the stochastically corroded steel fibre, indicating a high risk of corrosion. It is important to note that this scenario differs from the prior study, where both steel fibres were positioned adjacently along their length and exposed to an external AC disturbance, resulting in significant corrosion for both fibres [37]. Currently, ongoing research is to investigate the stochastic corrosion phenomena revealed in this investigation.

3.3 Numerical Modelling Results and Discussion

Section 2.3 discusses the boundary element modelling (BEM) approach used to validate the AC interference results presented in Sect. 3.2. The electric potential derived from BEM results is depicted as equipotential lines (or potential contour lines) alongside a current density vector (Fig. 16). Notably, distorted (noncylindrical) potential contour lines were observed in the region between the graphite electrodes and steel fibres, attributed to the narrow gap of 5 mm between them. The length of the arrows in the figure corresponds to the magnitude of the current density. When an electric current passes through the graphite electrodes, the embedded steel fibres become polarized, resulting in a potential difference (or voltage drop) between them. Figure 16 (a) shows that the maximum voltage drop between two steel fibres positioned back-to-back (position 1) was 1.4 V, closely aligning with the experimental measurement of 1.6 V. The voltage drop measured between the embedded steel fibres in the top-bottom orientation (position 2) was 3 mV, indicating a negligible voltage drop, consistent with the BEM modelling results shown in (Fig. 16 (b)) as well. The computer simulation approach used in this study has the potential to develop more valuable predictive tools for future research in similar research areas where electrical and electrochemical interactions are concerned.

Table 2 Tafel polarization results (after 1-hr AC interference)

		E_{corr} (mV)	β_a (V/dec)	β_c (V/dec)	i_{corr} ($\mu A/cm^2$)	CR (mm/year)
Position 1	Sample 1 (L)	-310	0.231	0.357	0.504	0.006
	Sample 1 (R)	-555	0.692	0.365	4.636	0.054
Position 1	Sample 2 (L)	-289	0.391	0.290	0.664	0.008
	Sample 2 (R)	-448	1.128	0.260	1.404	0.016
Position 2	Sample 1 (T)	-488	1.249	0.281	1.564	0.018
	Sample 1 (B)	-338	0.314	0.138	0.025	0.001
Position 2	Sample 2 (T)	-317	0.268	0.127	0.030	0.001
	Sample 2 (B)	-462	0.594	0.241	1.109	0.013

Note L: left; R: right; T: top; B: bottom

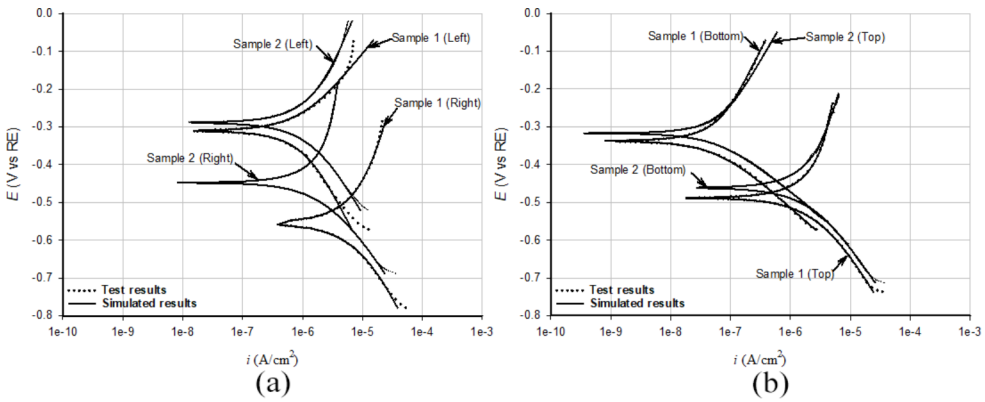

Fig. 15 Tafel polarization results after 1-hr AC interference (0.3 mol/L NaCl). (**a**) Position 1: back-to-back arrangement. (**b**) Position 2: top-bottom arrangement

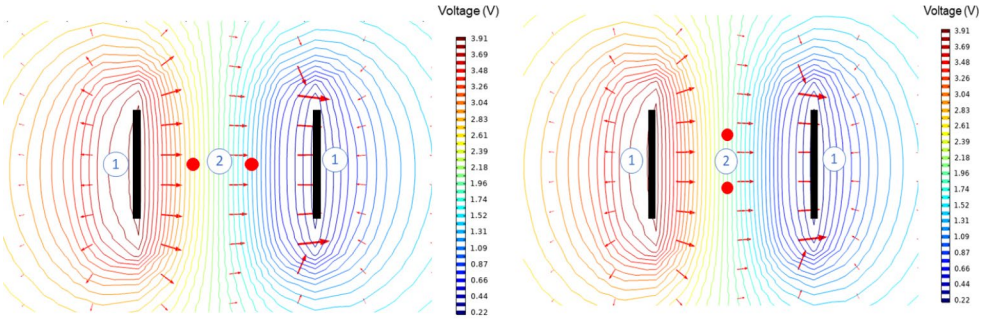

Fig. 16 BEM result – equipotential lines ($t = 0.005$ s). (**a**) Steel fibre position 1: back-to-back arrangement. (**b**) Steel fibre position 2: top-bottom arrangement

4 Conclusions

In this study, the cyclic potentiodynamic (CP) polarization technique was used to simulate stray DC interference. Steel fibres demonstrate good corrosion resistance to stray DC perturbations up to 1.0 V (vs. OCP), in the absence of chloride. With 0.6 mol/L chloride in the electrolyte, a reduced but still significant DC perturbation of 0.4 V (vs. OCP) was required to initiate pitting corrosion, indicating reduced corrosion resistance. A scanning rate of up to 5 mV/sec is suitable for evaluating the breakdown of the steel's passive layer in the presence of ample chloride ions (e.g. 0.6 mol/L) in the electrolyte. This finding is very important for future research involving the use of polarization techniques, as it enables more efficient investigations without compromising crucial and meaningful results at an accelerated scanning rate.

The AC interference test was conducted on two embedded steel fibres with two different orientations. After the 1-hour AC interference test, the Tafel polarisation test shows a stochastic corrosion pattern in the two embedded steel fibres. Notably, there is a significant decrease in the corrosion potential (E_{corr}) and a corresponding increase in the corrosion current density (i_{corr}) in only one of the two fibres. Ongoing research is to investigate the stochastic corrosion phenomena revealed in this investigation.

The boundary element modelling (BEM) approach was use in this study to validate the AC interference results. The electric potential derived from BEM was illustrated as equipotential lines (or potential contour lines) alongside a current density vector. The BEM results demonstrate that the maximum voltage drops between steel fibres positioned in different configurations closely match the experimental measurements. The computer simulation approach applied in this study has the potential to advance the development of more valuable predictive tools for future research in the realm of electrical and electrochemical interactions.

Notations

A	Exposed anode area of a working electrode (cm^2)
C_f	Steel passive layer capacitance CPE ($S{\cdot}s^n{\cdot}cm^{-2}$)
C_{dl}	Double layer capacitance CPE ($S{\cdot}s^n{\cdot}cm^{-2}$)
$E_{e,\,a}$,$E_{e,\,c}$	Anodic and cathodic equilibrium potentials (V)
E_{corr}	Corrosion potential (V)
E_0	Amplitude of the AC potential (V)
E_{pit}	Steel pitting potential (V)
E_{rep}	Steel repassivation potential (V)
EW	Metal mass oxidized per Faraday of electric charge (27.925 for steel)
K	Constant value 3.27×10^{-3} (mm·g/μA·cm·year)
I_0	Amplitude of the AC current (A)
I_a, I_c	Anodic and cathodic currents (A)
I_{corr}	Corrosion current (A)
i_{corr}	Corrosion current density (mA/cm^2)
i_{peak}	Peak current density (mA/cm^2) during CP polarization
η_a	Anodic overpotential (V)
ρ	Steel density (7.8 g/cm^3 for steel)
R_s	Resistance of the solution (Ω)
R_f	Film or membrane resistance (Ω)
R_{ct}	Charge transfer resistance (Ω)
ω	Angular velocity ($\omega = 2\pi f$, rad/sec)

Acknowledgements The author extends heartfelt gratitude to Lu, Fanyi, and Fanai, beloved family members, for their unwavering patience and steadfast support throughout these years. The author also expresses sincere appreciation to Colin Eddie, John Booth, and John Greenhalgh for their invaluable guidance.

References

1. Tang K (2017) Stray current induced corrosion to steel fibre reinforced concrete. Cem Concr Res 100:445–456
2. Tang K (2019) Stray alternating current (AC) induced corrosion of steel fibre reinforced concrete. Corros Sci 152:153–171
3. Bertolini L (2013) Corrosion of steel in concrete prevention, diagnosis, repair. Wiley-VCH, Weinheim, Germany
4. Kuang D, Cheng YF (2014) Understand the AC induced pitting corrosion on pipelines in both high pH and neutral pH carbonate/bicarbonate solutions. Corros Sci 85:304–310
5. Bertolini L, Carsana M, Pedeferri P (2007) Corrosion behaviour of steel in concrete in the presence of stray current. Corros Sci 49:1056–1068
6. Hanson HR, Smart J (2004) AC Corrosion on a Pipeline located in a HVAC Utility Corridor. Corrosion, NACE International, New Orleans, Louisiana
7. Mangat PS, Gurusamy K (1988) Corrosion resistance of steel fibres in concrete under marine exposure. Cem Concr Res 18:44–54
8. Jovičić V, Šušteršič J (2008) Use of fibre-reinforced shotcrete for primary lining in the Dekani tunnel. Quark, Summer, pp 112–117
9. Burgess M, Davies H (2007) Channel tunnel rail link Sect. 2: Thames tunnel, Proceedings of the Institution of Civil Engineers: Civil Engineering, 160 14–18
10. Lin L (2005) Study of the influence to the steel fiber concrete durability due to the stray current, MSc thesis, China University of Mining and Technology, Beijing
11. Michels J, Gams M (2016) Preliminary study on the influence of fibre orientation in fibre reinforced mortars. Građevinar 68:645–655
12. Caratelli A, Rivaz BD, Meda A, Rinaldi Z, Dubrovnik (2015) Croatia
13. Ozyurt N, Mason TO, Shah SP (2006) Non-destructive monitoring of fiber orientation using AC-IS: an industrial-scale application. Cem Concr Res 36:1653–1660
14. Wijffels MJH, Wolfs RJM, Suiker ASJ, Salet TAM (2017) Magnetic orientation of steel fibres in self-compacting concrete beams: Effect on failure behaviour. Cem Concr Compos 80:342–355
15. Xue W, Chen J, Xie F, Feng B (2018) Orientation of Steel Fibers in magnetically driven concrete and Mortar. Materials 11:170
16. Kang ST, Park JJ, Ryu GS, Kim SW (2008) Fiber Alignment of Steel Fiber Reinforced High Strength Concrete (SFR-HSC) in Flexural members and its Effect on the Flexural Strength. Key Eng Mater 385:789–792
17. Villar VP, Medina NF, Hernández-Olivares F (2019) A model about dynamic parameters through magnetic fields during the alignment of steel fibres reinforcing cementitious composites. Constr Build Mater 201:340–349
18. Tang K (2020) Corrosion of discontinuous reinforcement in concrete subject to railway stray alternating current. Cem Concr Compos 109:103552–103552
19. Tang K (2019) Corrosion of steel fibre reinforced concrete (SFRC) subjected to simulated stray direct (DC) interference. Mater Today Commun, 100564–100564
20. Ye CQ, Hu RG, Dong SG, Zhang XJ, Hou RQ, Du RG, Lin CJ, Pan JS (2013) EIS analysis on chloride-induced corrosion behavior of reinforcement steel in simulated carbonated concrete pore solutions. J Electroanal Chem 688:275–281
21. Poursaee A (2010) Corrosion of steel bars in saturated ca$(OH)_2$ and concrete pore solution. Concrete Res Lett 1:90–97
22. Wang W, Chen H, Li X, Zhu Z (2017) Corrosion behavior of steel bars immersed in simulated pore solutions of alkali-activated slag mortar. Constr Build Mater 143:289–297
23. Hausmann DA (1967) Steel corrosion in concrete. Mater Prot 6:19–23
24. Saremi M, Mahallati E (2002) A study on chloride-induced depassivation of mild steel in simulated concrete pore solution. Cem Concr Res 32:1915–1921
25. Brenna M, Dolara A, Leva S, Zaninelli D (2010) Effects of the DC stray currents on subway tunnel structures evaluated by FEM analysis, in: IEEE PES General Meeting, PES July 25, 2010 - July 29, 2010, IEEE Computer Society, Minneapolis, MN, United states, 2010, pp. 1–7
26. Cui G, Li Z-L, Yang C, Wang M (2016) The influence of DC stray current on pipeline corrosion. Pet Sci 13:135–145
27. Gamry GE, Analyst (2015) Gamry Instruments, Inc.
28. ASTM (1999) G102-89 standard practice for calculation of corrosion rates and related information from electrochemical measurements. American Society for Testing and Materials, West Conshohocken, PA
29. Wikipedia (2018) Skin effect
30. Bortels L, Dorochenko A, Bossche BVd, Weyns G, Deconinck J (2007) Three-dimensional boundary element method and finite element Method simulations Applied to Stray current interference problems. A unique coupling mechanism that takes the best of both methods, vol 63. Corrosion, pp 561–576
31. K S (2000) Influence of mixing vehicle on dissociation of calcium hydroxide in solution. J Endod 26:649–651
32. Golnabi H, Matloob MR, Bahar M, Sharifian M (2009) Investigation of electrical conductivity of different water liquids and electrolyte solutions. J Theoretical Appl Phys 3:24–28
33. Wikipedia (2018) Electrical resistivity measurement of concrete
34. Helmenstine AM (2018) Table of Electrical Resistivity and Conductivity
35. Esmailzadeha S, Aliofkhazraeia M, Sarlakb H (2018) Interpretation of cyclic potentiodynamic polarization test results for study of Corrosion Behavior of metals: a review, Protection of metals and Physical Chemistry of surfaces. 54:976–989
36. Concrete, Society (2015) Technical Report 44 Relevance of cracking in concrete to reinforcement corrosion, in, Concrete Society, Surrey, UK, pp. 4–7
37. Tang K (2020) Corrosion of Steel Fiber subjected to Stray current interference. ACI Mater J 117:99–111